Distance Control in Trapped Particle Optical Microscopy

Diploma Paper by

Magnus Berglund

LRAP-161

Lund, June, 1994

Abstract

This Diploma paper describes methods and control electronics for distance control in non-intrusive scanning near-field optical microscopy. This distance control is necessary due to the strong dependence of resolution on the distance between probe and sample in such a microscope. Two different measurement methods are investigated. A resistive method based on conductivity measurements is found to show significant long-term drifts making it unsuitable for distance control in its current status. A capacitive method features good linearity and excellent accuracy. The automatic control electronics for the capacitive method is also described. Measurements show excellent suppression of long-term temperature drifts and a 3.5 nm rms noise, for the apparatus.

Table of Contents

Page

1. Introduction

In this diploma work two different methods for accurate non-invasive measurements of small distances will be investigated. The best method will be implemented in a control system intended to stabilise the probe-sample distance in a non-intrusive scanned near-field optical microscope. The control system will be carried out in both analogue and digital hardware.

1.1. Overview

The ordinary visible light microscope has a resolution that is limited to a few hundred nanometers due to far-field diffraction[1]. Since there are many structures that are smaller, e.g., viruses, proteins, it is most desirable to achieve a higher resolution. Basically there are two ways of doing this.

Since resolution is proportional to the wavelength, one way is to use a shorter wavelength. This is the principle of soft X-ray microscopes[2] and electron microscopes[3]. There are a few problems when using x-rays. Very-high resolution x-ray microscopy on biological materials is difficult due to the radiation damage caused by high energy photons. Furthermore optics in this wavelength regime is inefficient. When using electron microscopy the sample has to be dehydrated, stained, fixed, sectioned and in vacuum. This makes it impossible to use on living biological material.

The other way is to use a scanned probe method, e.g., Atomic Force Microscopy (AFM)[4], Scanning Tunnelling Microscopy (STM)[5] or Scanned Near-Field Optical Microscopy (SNOM)[6]. Here the idea is to scan a small probe (small compared to the resolution limit, i.e., 200 nm) over the sample.

1.2. Trapped particle optical microscopy

Trapped Particle Optical Microscopy (TPOM)[7,8,9] is a SNOM related technique. The basic principle is to use an optically trapped microscopic particle as a sub-wavelength light source probe, cf. Fig 1.1.

The particle used is a frequency doubling crystal made of lithium niobate or potassium titanyl phosphate (KTP). When using a Nd:YAG laser with 1.06 μm wavelength, the frequency-doubled light will be 532 nm. By separating the trapping and detection wavelength, two advantages are gained. Infrared light exhibits a low absorption in most biological materials, thereby minimising the thermally induced damage in the studied object. Scattered infrared light can be filtered out and will not interfere with the detection of the 532 nm light. The main advantage of the TPOM is its non-intrusive probe. It can for instance be used with intervening membranes and will also allow tip-sample collisions without any damage. Both features are unique in a scanned probe method. Since it works in water and with moderate trapping beam intensities (≈100 mW) it can be used on living biological materials.

Due to the $1/r^2$ dependence of the emitted intensity from the particle, the object should be in immediate proximity to the probe particle, i.e., much closer than one wavelength, in order to achieve high resolution. If this is done the resolution mainly depends upon the effective size

of the particle, i.e., the physical size of the trapped particle convolved with its displacement due to Brownian motion, and on the distance between the sample and the probe[7].

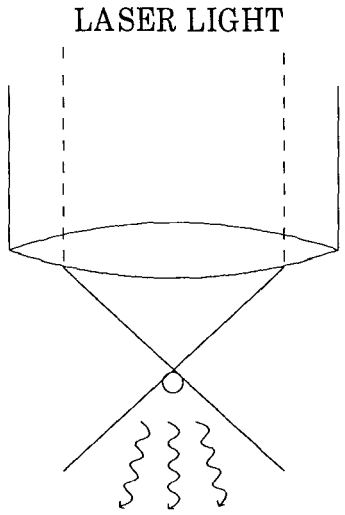

Fig. 1.1. The TPOM principle.

This distance varies due to thermal expansions in the experimental arrangement and due to low-frequency vibrations caused by, e.g., the ventilation or heating systems. Figure 1.2. shows a vibration measurement made on the optical table that is used in the TPOM experiments[10].

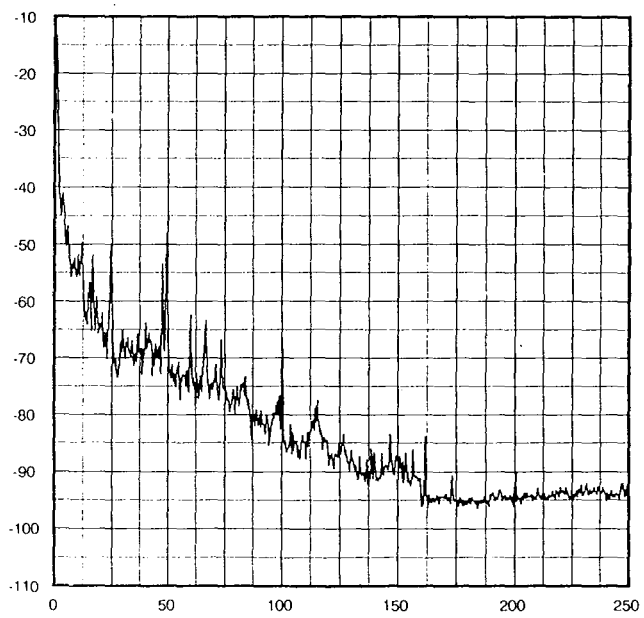

Fig. 1.2. A vibration measurement. The horizontal axis is the frequency (Hz) and the vertical is the displacement relative 1 μm, i.e., -20 dB equals 100 nm, -40 dB equals 10 nm.

1.3. Distance control

In order to keep the probe-sample distance fixed we need a method to measure small distances very accurately and some kind of feedback to control the distance. In this diploma work we have set the maximum allowed distance displacement to 20 nanometers peak to peak. In Fig. 1.2 we can see that this requires a bandwidth of approximately 2 Hz.

In STM the distance is controlled by measuring the tunnel current between the tip and the sample. This can not be used in TPOM because it requires a conducting sample and a very small tip-sample distance. The first is not possible since we are dealing with biological samples and the latter would ruin one of TPOM's greatest advantages, namely the non-intrusive probe.

AFM uses the atomic forces between tip and sample to measure and control the distance. These forces are only measurable when the distance is very small and therefore this method can't be used.

Initially a method based on measurement of conductivity was evaluated. Since the TPOM works in isotonic solution, i.e., approximately 0.8% sodium-chloride in water, this method would be preferable. However, due to electrode contamination the long-term drift of this method could not be controlled. In Section 2.1. the principles and limitations of conductive measurements are discussed. One well known way to measure small distances very accurately is to use a capacitive bridge method[11]. This requires a high resistive medium and can therefore not be used in water. In Section 2.2 this method is further investigated and it is found that a resolution of 2.5 nm is achievable. In Chapter 3 an automatic-control unit is developed based on the capacitive bridge method in air. A solution to the problem with combining air measurements and the demand to work in water is presented in Section 3.1.1. Further it is found that the constructed control unit is able to stabilise low-frequency vibrations and long-term drifts. Finally in Chapter 4 a few improvements are discussed and two alternative methods are proposed.

2. Methods

In this Chapter the principles of the resistive and capacitive distance measurement methods are discussed. In both experiments the electrodes were made of brass and platinum with circular geometry. The diameter was 5 mm for brass and 3 mm for the platinum electrodes. The experimental arrangement is shown in Fig 2.1. For xyz motion a piezo electric driven stage (Photon Control Microblock) was used.

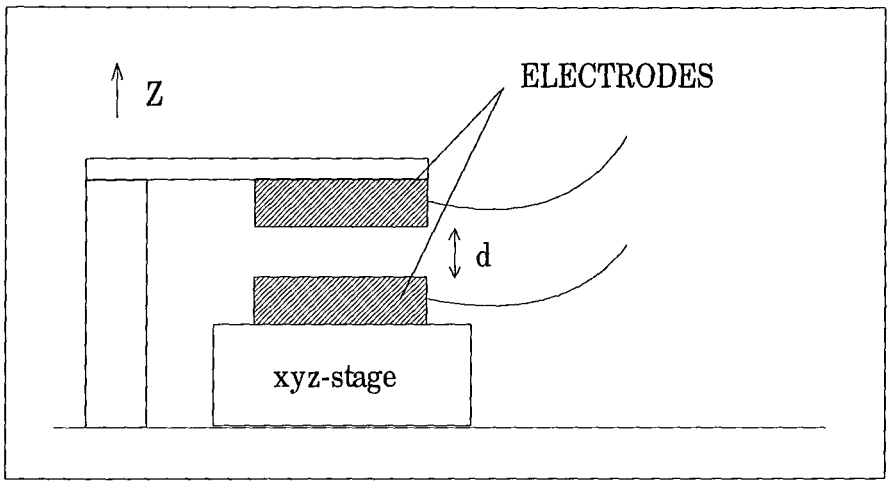

Fig. 2.1. The experimental arrangement.

2.1. Resistive method

2.1.1. Theory

The resistance between two parallel electrodes as in Fig 2.1 is

$$R = \frac{d}{\gamma \cdot A}, \qquad (2.1)$$

where d is the distance between the electrodes, A the electrode area and γ the conductivity (12.9 mmho/cm in 0.8 % NaCl solution[12]). An electrode distance of 100 microns and an electrode area of $2 \cdot 10^{-5}$ m^2 results in a resistance of 4 Ω. The most accurate way to measure this resistance is to use a bridge technique[13], cf. Fig. 2.2. To avoid ion drift AC voltage was used. When applying a voltage between the electrodes this will create an electrical double layer in the sodium chloride solution near each electrode[14]. This double layer can be modelled as a capacitance. A model of the electrodes is shown in Fig. 2.3. With a given potential

difference this double layer has a capacitance between 10-40 $\mu F/cm^2$ [15]. This capacitance depends on the applied voltage. The total impedance will then be

$$Z = \frac{1}{j \cdot \omega \cdot C} + R + \frac{1}{j \cdot \omega \cdot C} \qquad (2.2)$$

By simply using a high frequency the capacitive part can be neglected and the resistance can be measured. If for instance 100 kHz is used the capacitive part will only be 7% of the total impedance.

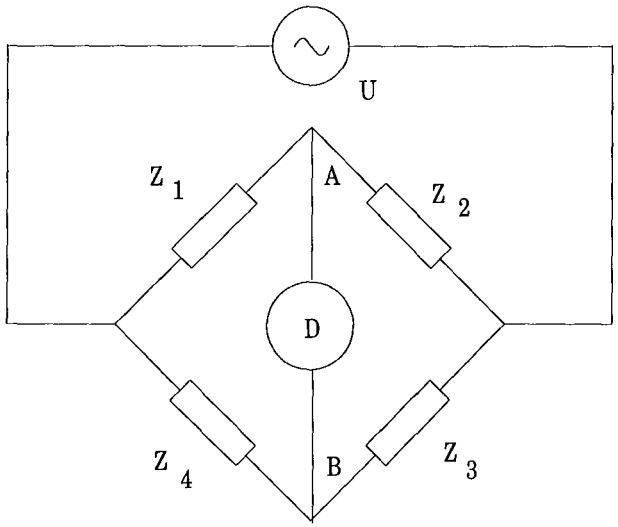

Fig. 2.2. The bridge technique.

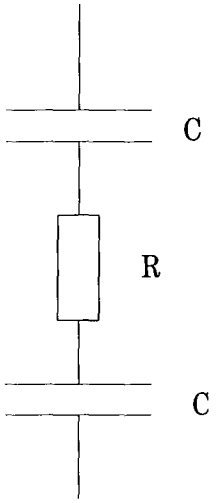

Fig. 2.3. A model of the electrode system.

2.1.2. Experiments

To confirm Eq. (2.2), the absolute value of Z was measured using different frequencies. The result is presented in Fig. 2.4. As can be seen the measurements agrees quite well with theory. When using the brass electrodes a resolution of 25 nm due to noise (> 2 Hz) was achieved but a long-term drift was also present. This drift can be explained by the reaction between chloride from the solution and copper from the electrodes. This was confirmed by observing a green deposit on the electrodes. I was then advised[16] to use platinum electrodes instead. With these electrodes the drift decreased but still it was to high to be explained by temperature expansions.

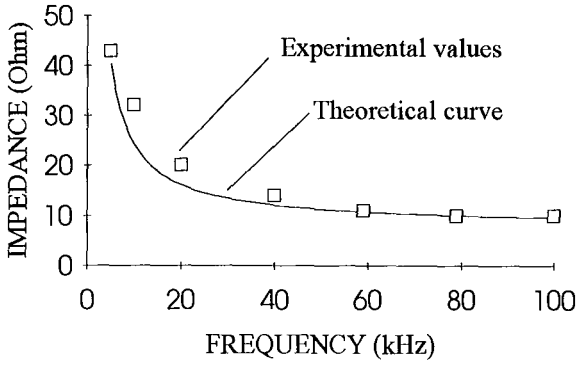

Fig. 2.4. A verification of Eq. 2.2.

2.1.3. Discussion

Platinum is known to be very inert and this is indeed true. But biological material still causes reactions with platinum as catalyst and the TPOM is meant to be used in biological applications. There are a lot of different methods to clean the electrodes available, e.g., electrolysis or alkali cleaning, but none is easily performed without damaging the microscope lens, cf. Sect. 3.1.1. Since this cleaning will have to take place at least once every hour[16] the resistive method in its current status is not a suitable distance control method for the TPOM.

2.2. Capacitive method

In this method the two electrodes are looked upon as a plate capacitor.

2.2.1. Theory

The capacitance between two plates, each with an area of A, parted a distance d is well known to be

$$C = \varepsilon_r \cdot \varepsilon_0 \cdot \frac{A}{d} \ , \tag{2.3}$$

where ε_0 is the vacuum permittivity ($8.85 \cdot 10^{-12}$ As/Vm) and ε_r is the relative permittivity which is 80 in water and 1 in air. A small increase of d with Δd will then change C according to

$$\frac{\partial C}{\partial d} = -\varepsilon_r \cdot \varepsilon_o \cdot \frac{A}{d^2} \quad \Rightarrow \quad \Delta C = \varepsilon_r \cdot \varepsilon_0 \cdot \frac{A}{d^2} \cdot \Delta d \, . \tag{2.4}$$

This results in a linear dependence between the change in capacitance and in length for small changes. The capacitance can be measured with a capacitance meter (I have used a Boonton model 72 BD) or with a bridge technique according to Fig. 2.2. The Boonton meter has a resolution of 1 femtofarad. With Eq. (2.4) and $A = 2 \cdot 10^{-5}\,m^2$, $d_0 = 50\,\mu m$ this results in a maximum resolution of 14 nm in air and 0.18 nm in water. Thus air measurements with the commercial meter may not be sufficiently accurate. By using a capacitive bridge method better accuracy can be obtained. One disadvantage when using capacitors in all four arms in the bridge is that it is not possible to measure the absolute value of capacitance (due to stray capacitances), but since we are only interested in changes of the length for the distance control, this will not be a problem. The bridge was driven by a 10 kHz, 2V peak to peak voltage from the internal oscillator in the lock-in amplifier (EG&G model 5209). The same amplifier was also used to measure the voltage difference between the two points A and B in Fig. 2.2. The change of this voltage difference is proportional to the change in capacitance when assuming small changes according to Appendix A. Parallel to the voltage input on the lock-in amplifier there is a capacitance of 25 pF. If we take this in account and also consider that the coaxial cables used to connect A and B to the lock-in amplifier and the cables used to connect the electrodes to the bridge has a capacitance of 50 pF and 10 pF, respectively, we get a more realistic model. All these capacitors are parallel to the original four. To get the sum of two parallel capacitors we simply add them and the main problem with these unwanted capacitors is that they will make the bridge less sensitive. Due to a higher temperature coefficient in the coaxial cables the bridge will also be less stable with respect to temperature changes.

2.2.2. Experiments

At first the linearity of the piezo electrically driven stage was investigated. This was done by mounting a digital length gauge (model Heidenhain MT12B with a resolution of 50 nm) on top of the xyz stage. The voltage applied over the piezo can be varied with an amplifier between 0-150 V. A plot is presented in Fig. 2.5. As we can see, the linearity is quite good in the middle, at each end the curve is slightly bent due to hysteresis. Here it was noted that when changing the voltage say 10 V most of the length change came immediately but the last 200-300 nm took as long as five minutes to settle. This phenomenon is hard to explain but it should not cause any problems since the feedback control unit will compensate for this.

To verify Eq. (2.3) and (2.4), capacitive measurements were made in air using the Boonton capacitance meter. The results are shown in Fig. 2.6 and 2.7. In both measurements the electrode distance was calibrated using 50 μm and 100 μm thick foil metals. The small discrepancy between the first series (up to 0.02 μm^{-1}) and the second in Fig. 2.6 is probably due to calibration difficulties. With the help of the Heidenhain length gauge different calibrations showed a calibration error of approximately 5 μm. Taking this into account the Figures shows an excellent linearity and full agreement with theory, which seems applicable to our model.

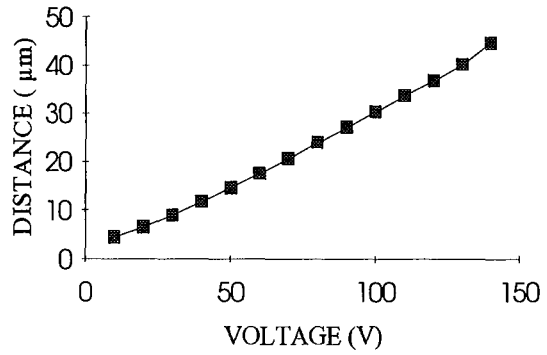

Fig. 2.5. Xyz-stage linearity.

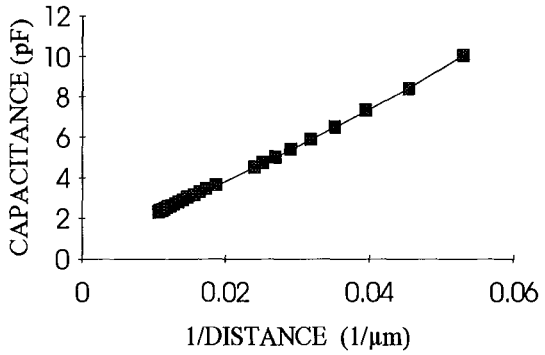

Fig. 2.6. Experimental verification of Eq. (2.3).

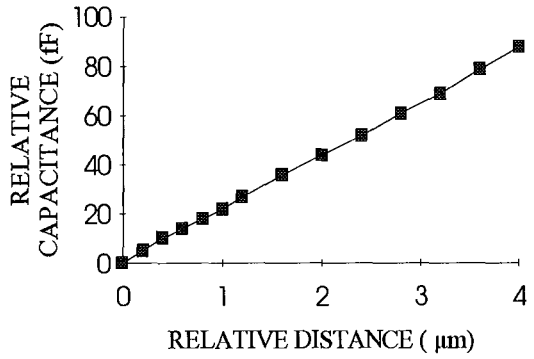

Fig. 2.7. Experimental verification of Eq. (2.4).

2.2.3. Discussion

The capacitive method has the disadvantage of not working in water due to its conductivity. Since water operation is not an absolute demand and because of the difficulties with calibration and cleaning using the resistive method, the capacitive approach will be used for the distance control system. With the commercial capacitive meter the resolution might be a problem since it is not possible to make the electrode area much larger and thereby increasing the capacitance change, according to Eq. (2.4). Therefore the bridge technique will be used.

3. Distance Control System

An overview of the experimental arrangement for the distance control system is shown in Fig. 3.1. The relative distance is measured with the capacitive bridge and detected with a lock-in amplifier. The amplifier output is fed into a PI-controller and a digital hold circuit. The hold circuit generates a reference signal for the controller. This signal is set manually through the adjust/hold switch. Finally, the PI-controller adjusts the distance through the piezo-electric xyz-stage.

The capacitive bridge is further discussed, in Sect. 3.1. There is also a discussion about automatic control theory and about proportional and integrating controllers in Sect. 3.2. In Sect. 3.3 a sample and hold circuit is constructed using digital components. Finally in Sect. 3.4 measurements are made showing that the constructed control unit is capable of compensate for low-frequency vibrations and slow drifts. In the text there will be a few references to integrated circuits, e.g., IC3. These are found in Appendix B which contains a layout of the electronics.

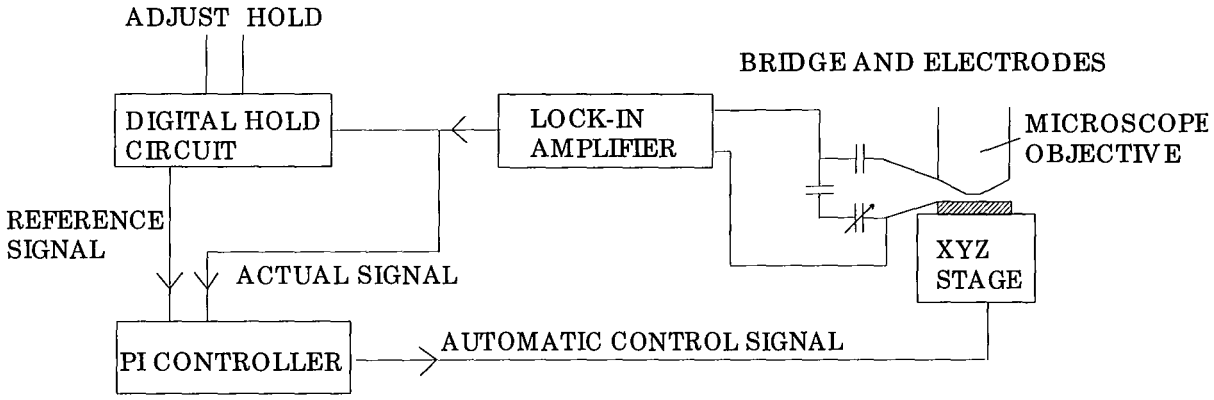

Fig. 3.1. The experimental arrangement.

3.1. The Bridge and electrodes

3.1.1. Design and construction

According to Chapter 2 the best method is the capacitive bridge, which requires a non-conducting medium. However in order to work, the TPOM has to be in water so one possible design of the microscope slide is proposed in Fig. 3.2. In the z direction there is a circular geometry. The inner ring works as a barrier to keep the water in and the outer one is used as one of the electrodes to measure the capacitance. The other electrode consists of the microscope objective. When this diploma work was carried out the microscope was still under construction so the final design of the microscope slide is still open. In this work a model similar to the one in Fig. 3.2 was used. The angle of the lower electrode was made to fit the

objective. With this geometry scanning in x or y direction will cause a capacitance change according to Appendix C. With a maximum scan of 5 μm this change will look like a distance change of 23 nm. This can be circumvented by using a design according to Fig. 3.3. The upper ring electrode is here glued on the microscope objective.

The capacitive bridge resembles Fig. 2.2, where Z_2 is the two electrodes and Z_1 is an adjustable capacitor with a range between 0 - 28 pF and a 30 ppm/K temperature coefficient. This adjustable capacitor is used to make $V_A \approx V_B$ as discussed in Appendix A. In the two arms with fix values (Z_4 and Z_3) there are ordinary capacitors with a temperature coefficient of 30 ppm/K.

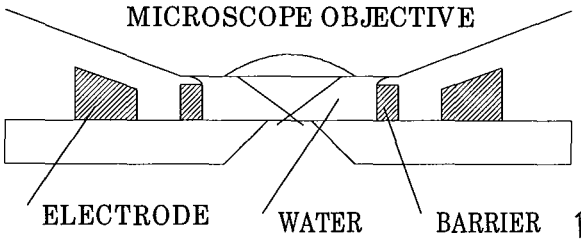

Fig. 3.2. A possible microscope slide design.

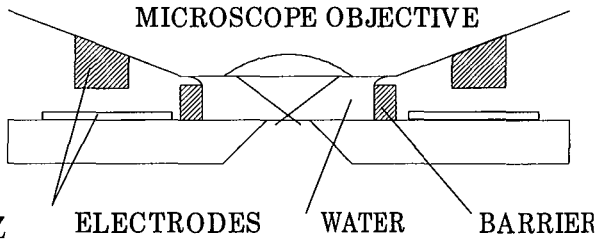

Fig. 3.3. A better design without scanning problems.

3.1.2. Temperature stability

To investigate if the bridge itself is temperature stable, the electrodes where substituted with a fixed capacitor. A drift corresponding to 5 nm/K was observed. This can be explained by changes in the coaxial cable or in the lock-in amplifier and it will limit the working range to four degrees (K). This is not a big problem since the temperature in the lab stays within four degrees. When connecting the electrodes, a small drift was present. This drift is correlated to the room temperature as can be seen in a long-term measurement in Fig. 3.4 and 3.5. This change is caused by thermal expansions in the experimental arrangement. According to Eq. (2.3), the capacitance depends on the electrode distance, the electrode area and the relative dielectric constant. Due to the large expansion in the experimental arrangement it is hard to investigate if the electrode area and ε_r changes and thereby affects the resolution. The electrodes are made of stainless steel with an expansion coefficient of $(1.15 \cdot 10^{-5}/\mathrm{K})$[17]. A temperature increase of one Kelvin will then change the area to $A' = A_0 \cdot (1.0000115)^2$ where A_0 is the original area. The capacitance is proportional to the area and will therefore change with the same factor. Combining Eq. (2.3) and (2.4) this results in $\frac{\Delta C}{C} = \frac{\Delta d}{d}$. Thus, the change in capacitance will result in an apparent distance change of $\Delta d = \frac{A' - A_0}{A_0} \cdot d = 2.3 \cdot 10^{-5} \cdot 50 \cdot 10^{-6} = 1.2$ nm. By simply replacing the steel electrodes with Zerodur, which hardly expands at all[18], this problem can be avoided. It is difficult to estimate the effects of variations in humidity and temperature on the relative dielectric

constant but since only small variations are of concern it is unlikely that changes in ε_r will be significant[19].

In order to study the short term fluctuations a five second measurement was made using a time constant of 1 ms, cf. Fig. 3.6. As can be seen, the noise level is 3 nm peak to peak. This corresponds to a change in capacitance of 0.2 fF. It should be noted that this recording was made with the piezo electric crystal turned off. When the piezo is on a noise of approximately 10 nm peak to peak is observed. This is caused by the amplifier which provides the crystal with a voltage. This amplifier has an output noise of 10 mV rms according to the manual and this corresponds to fluctuations of 9 nm peak to peak assuming a sinusoidal noise.

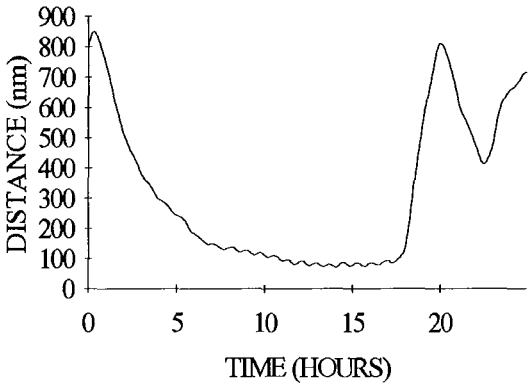

Fig. 3.4. A long term measurement

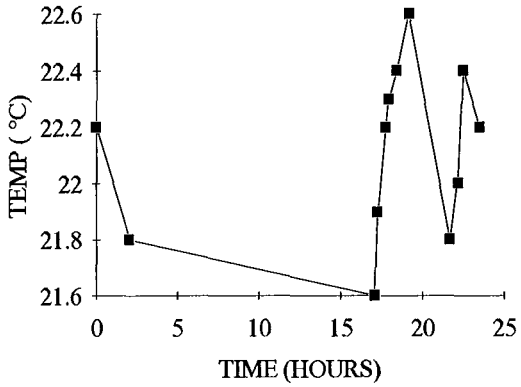

Fig. 3.5. The corresponding temperature.

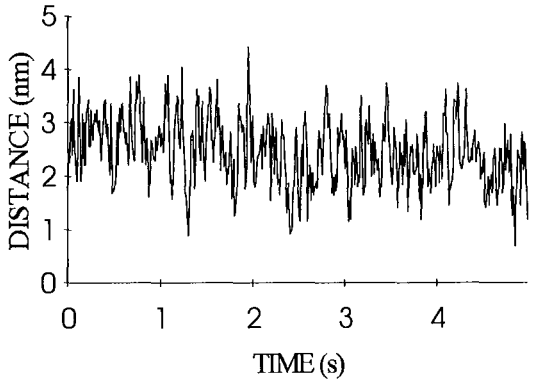

Fig. 3.6. Short-term noise recorded during 5 seconds .

3.2. The PI-controller

3.2.1. Theory

In order to have a fixed distance between the upper electrode (the microscope objective) and the lower electrode, which is integrated in the microscope slide, some kind of feedback system must be used. A natural choice is the proportional and integrating controller[20]. The derivative part is left out because of its sensitivity to high frequency noise. The basic idea of a PI-controller is to take the difference between a reference signal and the actual output signal. This difference is called the error signal and it is a measure of the deviation from the ideal state. After amplification and integration in the PI-controller this signal is used as input signal to the controlled system. A schematic picture is illustrated in Fig. 3.7.

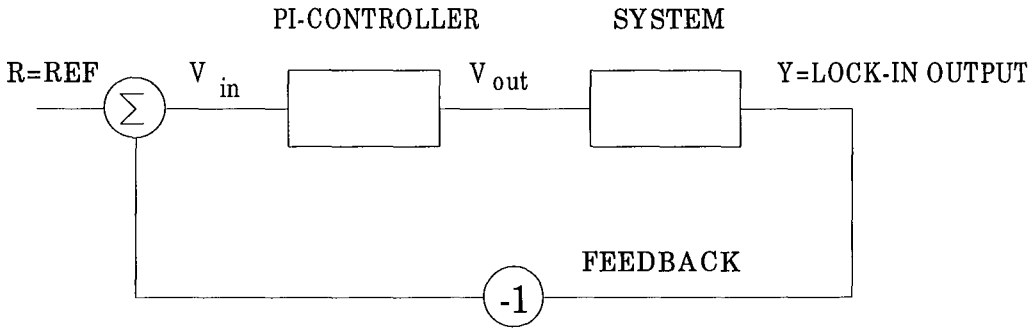

Fig. 3.7. A schematic picture of the feedback system.

The control law of a PI-controller is given by[20]

$$V_{out}(t) = K \cdot \left[V_{in}(t) + \frac{1}{T_i} \cdot \int_0^t V_{in}(\tau) \cdot d\tau \right] \tag{3.1}$$

Here the integrating part exists because a controller with only proportional part cannot remove a steady state error[20]. An increase of the amplification factor K results in a faster system which leads to a higher bandwidth. With a too large amplification, the system will be instable. An increase of the integrating part, i.e., a decrease of the time constant T_i, results in a faster response to steady-state errors but on the account of a poorer stability.

One popular way to determine K and T_i is the Zieger-Nichols method[20]. First you turn of the integrating part (setting T_i to ∞). Then you increase K until the system starts to oscillate. This value we call K_0 and the oscillating period T_0. According to Zieger-Nichols, the settings should then be $K = 0.45 \cdot K_0$ and $T_i = \frac{T_0}{1.2}$. These values could then be fine tuned in order to trim the system response.

The system to be controlled consists of the piezo amplifier, the micro-block xyz stage and the lock-in amplifier. Our input signal is the control signal to the piezo amplifier (0-5 V) and our output signal is the output value from the lock-in amplifier. This output has a range between +/- 10V. The slowest part in the system is the lock-in amplifier. If we ignore the dynamics in the microblock (it is much faster than the lock-in) then we can view the system as a simple time delay. This was verified by connecting a sinusoidal wave to the piezo amplifier input and observing the lock-in output on an oscilloscope together with the input. The output was not distorted but delayed. The delay depends on the lock-in time constant. When using the smallest time constant, a delay of 2 ms was obtained. This will cause a resonance at 250 Hz which was also experimentally verified. A time-delaying system is viewed in Fig. 3.8.

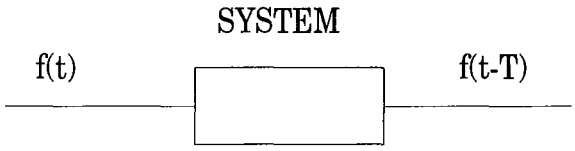

Fig. 3.8. A time-delaying system.

Systems containing long time delays are hard to stabilise but if the system has a known behaviour a Otto-Smith controller can be used[20]. This has a built-in correction to the time delay. Because of the fact that this time delay is hard to realise in analogue technique and since we do not need a very fast system, we will settle with the PI-controller. If Eq. (3.1) is Laplace-transformed we will get the control-law in the frequency domain

$$G_{PI} = K\left(1+\frac{1}{T_i \cdot s}\right), \tag{3.2}$$

where $s = i \cdot \omega = i \cdot 2 \cdot \pi \cdot f$ and f is the frequency. Likewise the time delay will cause a multiplication with

$$G_{sys} = e^{-s \cdot T} \tag{3.3}.$$

The open circuit (without feedback) will then be

$$Y = K\left(1+\frac{1}{T_i \cdot s}\right) \cdot e^{-s \cdot T} \cdot R = G_o \cdot R \ . \tag{3.4}$$

Here G_o is called the loop gain, R is the reference value and Y is the lock in output signal. If the feedback is taken into account the closed loop circuit will be

$$G_c = \frac{G_o}{1+G_o}. \tag{3.5}$$

The absolute value of this factor should theoretically be one but practically it will be a decreasing function of frequency. The frequency at which $|G_c| = \frac{1}{\sqrt{2}}$ is called the bandwidth and it expresses the ability to follow changes in the reference signal. A plot of $|G_c|$ with K and T_i determined according to Zieger-Nichols method is presented in Fig. 3.9. As we can see the theoretical bandwidth is approximately 50 Hz.

The sensitivity function is defined as

$$S(s) = \frac{1}{1+G_o(s)}. \tag{3.6}$$

It expresses how the output signal is influenced by outer disturbances. If S is small we will have a good disturbance rejection. A plot of $|S(f)|$ is presented in Fig. 3.10 and 3.11. As expected the low frequency disturbances are taken care of by the integrating part but higher frequencies can not be corrected entirely due to the time delay. The sensitivity function is more interesting than the bandwidth in our case and from Fig. 3.11 it can be noted that disturbances at 2 Hz will be damped to 0.05 of its original value.

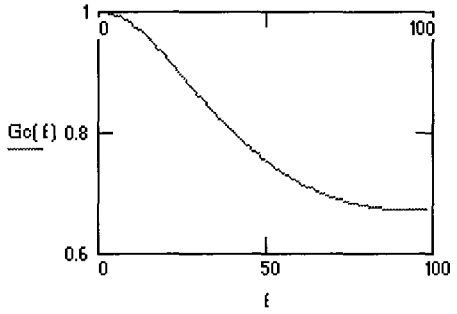

Fig 3.9 The closed loop amplification versus frequency.

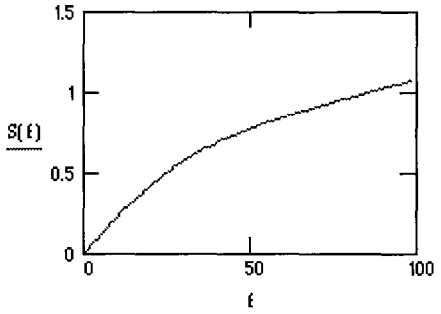

Fig 3.10 The sensitivity function versus frequency.

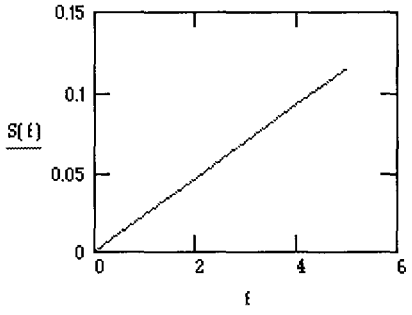

Fig 3.11 The sensitivity function in the low-frequency regime.

3.2.2. Design and construction

The different parts of a PI-controller can be constructed using operational amplifiers[21,22] as depicted in Fig. 3.12.

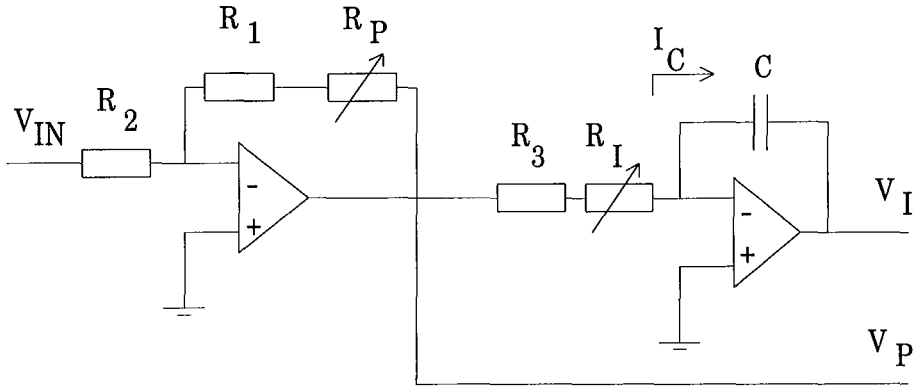

Fig. 3.12. The PI-controller.

The proportional section consists of an inverting amplifier (IC4 in Appendix B) with the gain

$$K = -\frac{R_1 + R_P}{R_2} \quad . \tag{3.7}$$

The following equation is valid for a capacitor

$$I_C = C \cdot \frac{dV_C}{dt} \quad \Rightarrow \quad V_C(t) = \frac{1}{C} \cdot \int_0^t I_C(\tau) \cdot d\tau \quad . \tag{3.8}$$

Assuming an ideal operational amplifier (IC5) both inputs must have the same potential (in our case zero).

Therefore

$$V_P = (R_3 + R_I) \cdot I_C \qquad \text{and} \qquad V_I = -V_C = -\frac{1}{C \cdot (R_I + R_3)} \cdot \int_0^t V_P(\tau) \cdot d\tau \tag{3.9}$$

with the time-constant $T_i = (R_3 + R_I) \cdot C$.

When adding these two signals we will arrive at the control law for a PI-controller Eq. (3.1). This is done by IC6 where the adjustment voltage also is added.

3.3 The Hold circuit

To store the reference value it will be needed some kind of hold circuit. This circuit should be able to hold the reference voltage for at least one hour. Due to leak currents it is not possible to store a voltage that long using analogue technique. Instead it was realised using an analogue to digital converter (ADC) model HI 5812JIP (IC7) and a digital to analogue converter (DAC) model PM 7541 (IC8) as shown in Appendix B. Thus the analogue reference value is stored digitally in the internal digital memory of the ADC and the DAC continuously provides a correct analogue reference value. Both components use twelve bits which gives 2^{12}=4096 different values between max. and min. With a reference voltage of 4.6 Volts this means a resolution of 1.1 mV. This voltage is maintained with a voltage reference model LM 385Z which has a drift of 200 ppm/K. With 4.6 V this results in a drift of 0.9 mV/K. From the lock-in output there is 10 mV per 2.5 nm (determined experimentally) and this voltage is divided by two and limited to positive values before reaching the ADC. This is done because the ADC has a maximum input of 5V. There is also a follower (a unity gain amplifier) IC1 before the ADC to create a low impedance signal. This is important when using an adder as IC3.

On each output on the ADC there is a built in latch. A latch is a digital component which has two inputs and one output. When one of the inputs is high (the sample/hold signal) the output will follow the input but when setting the sample/hold signal low the output will freeze. By connecting the ADC outputs directly to the DAC inputs we have a circuit which follows the input when a sample/hold signal is high and freezes the output on the last received input voltage when setting the signal low. This is a sample and hold circuit with unlimited hold time.

The output from the DAC is inverted by an inverting unity gain amplifier IC2. To create the error signal it is simply to add the DAC output and the output from the lock-in amplifier. This is done by IC3.

3.4. Measurements

In order to test the control-unit a few experiments were conducted.

3.4.1. Bandwidth

To create periodic vibrations, a loudspeaker was mounted on the experimental set-up. This speaker was only able to reproduce vibrations down to 20 Hz. At this point the system was able to reduce the vibration to 0.4 of its original value. At 100 Hz the system made the signal a bit stronger, approximately 1.05 of the original value. This and other measurements between 20 and 200 Hz also agrees with theory according to Sect. 3.2.1.

3.4.2. Temperature stability

To test the ability to stabilise temperature expansions a measurement with various temperatures was made. In Fig. 3.13 and 3.14 the results are shown. The temperature was measured in the air close to the experimental set-up. In the first part the control-unit was in adjust mode. In this mode the PI-controller is not connected. In the second part it was in hold mode, i.e., the PI-controller is active. It can be seen that the system is capable of stabilising slow changes of the distance. It can also be seen in Fig. 3.14 that the reference value was stable and did not change due to temperature. This is as expected according to theory in Sect. 3.3. The noise level can be approximated from Fig. 3.14 to 10 nm peak to peak, i.e., the rms noise is approximately 3.5 nm.

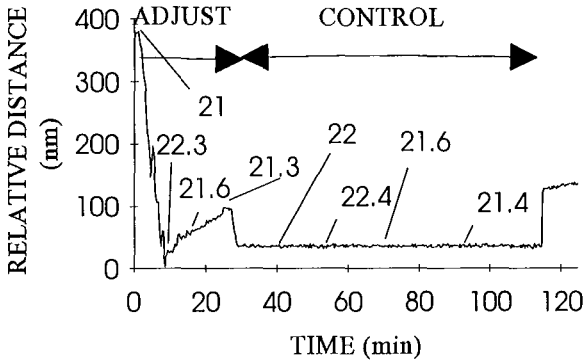

Fig 3.13. A test of the control-unit.

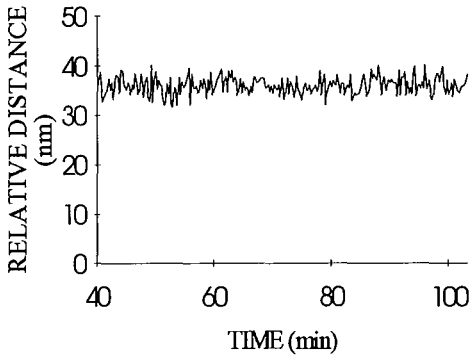

Fig 3.14. A close-up of fig 3.12.

4. Conclusions and Future Work

A system has been constructed, able to measure a distance of 50-100 μm with a resolution of 2.5 nm peak-to-peak. A proposal of how to integrate the system with a TPOM has also been made. In order to stabilise the distance a PI-controller has been constructed. As has been shown the system is able to compensate for slow changes such as those due to low-frequency noise and temperature changes. The current system bandwidth is 50 Hz due to the time-delay in the lock-in amplifier and the short-term noise is 10 nm peak-to-peak (3.5 nm rms) due to noise in the amplifier driving the piezo-electric stage. The current arrangement also has a systematic error in the order of 10-20 nm due to the angled electrodes, cf. Appendix C. However, this error may easily be eliminated by changing the electrode design. A manual to the control-unit is found in Appendix D.

To be able to increase the bandwidth a lock-in amplifier with a smaller time-constant must be constructed. The microblock need to be exchanged to one with an even faster response. To decrease the noise level, a piezo amplifier with a lower output noise is needed and to extend the working temperature range the bridge components and the coaxial-cables have to be more precisely matched.

In this work changes of the capacitance in the order of 0.2 fF was measured. Today's state-of the-art is at 0.1 aF[23]. Thus, an increase of the resolution in this system should not be impossible.

The main disadvantage with this system is that it does not work in water. This would have been preferable as it makes the microscope design easier. During this work two methods that might work in water has turned up. The first is the already investigated capacitive method. In order to avoid reactions on the electrodes and also to limit the current, the electrodes should be covered with a thin foil of PTFE[23]. One disadvantage with this method would be that the foil has to be thin and therefore fragile. The other is a interferometric method where a fiber is used as a Michelson interferometer with both arms in the same fiber[24], as shown in Fig. 4.1 and 4.2. The reflection in the end of the fiber is used as one beam and the reflection in the upper electrode is used as the other. Eventually a graded index lens (GRIN) could be used to focus the light and thereby increase the amount of recollected light.

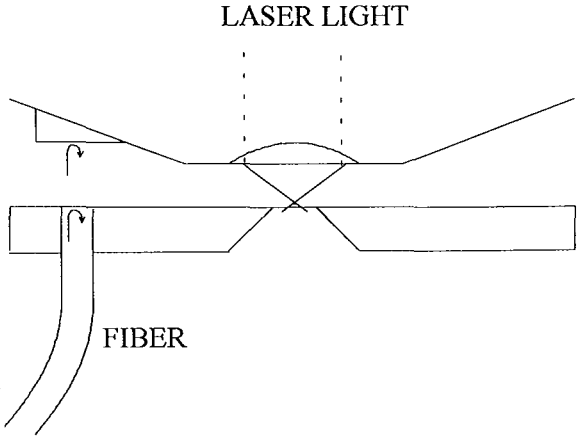

Fig 4.1. A fiber interferometer.

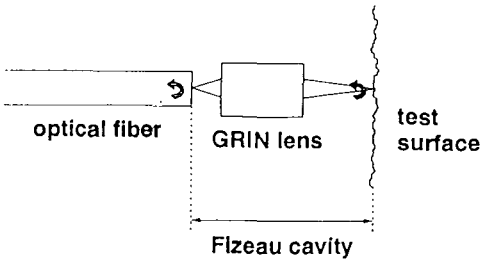

Fig 4.2. Using a GRIN lens to focus the light (from Ref. 24).

5. Acknowledgements

I would like to thank all the people that work at the Division of Atomic Physics in Lund. Especially I would like to mention:

My supervisor Hans Hertz, who outlined this project and helped me throughout my work. He has provided great knowledge and inspiration. Thank you.

Lars Malmqvist and Lars Rymell, they have helped me with a great number of problems, both practical and theoretical.

Åke Bergquist and Bertil Hermansson at the electrical workshop. Without their help I would still be trying to make the electronics work.

Jan Hultkvist at the engineering workshop. He has been very helpful and made the project run smooth.

From outside the Division I would like to thank:

Gillis Johansson and Christine Berggren-Kriz at the Department of Analytical Chemistry, Lund, for taking the time to teach a novice a few things about electrochemistry and platinum electrodes.

P. O. Sjöstrand, at the Department of Electrical Measurements, Lund, who provided valuable test equipment.

Gert Inge Bertilsson at Gambro, Lund, for providing useful information about platinum electrodes.

Appendix A

Calculation of the dependence between a small change in measured capacitance Z_2 and the change in voltage V_A.

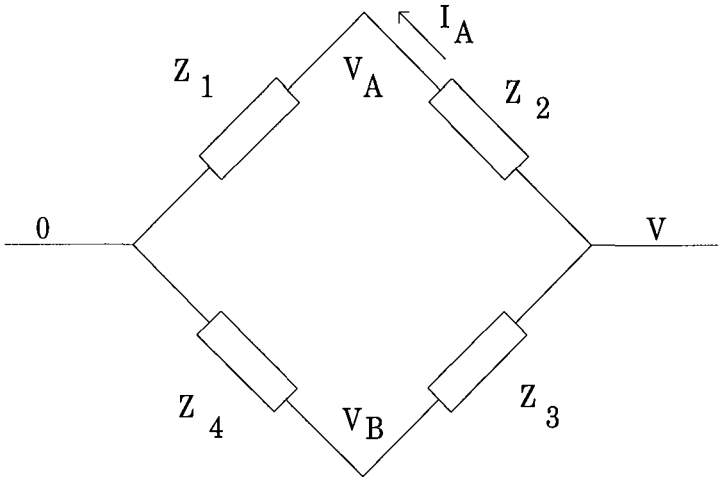

Fig. A1. Capacitive bridge.

Assuming the electrodes are placed at Z_2, the lower arm is only used to create a stable voltage V_B approximately as large as V_A. By doing this, the difference between A and B is small and can be measured very accurately with a lock-in amplifier in difference voltage mode..

Initially we have

$V_A = Z_1 \cdot I_A$ and $V - V_A = Z_2 \cdot I_A$ this gives

$$V_A = \frac{V}{1 + \frac{Z_2}{Z_1}} \quad \text{and in the same way} \quad V_B = \frac{V}{1 + \frac{Z_3}{Z_4}}.$$

If a small change in capacitance is introduced this will lead to a change in impedance according to

$Z_2' = Z_2 + \Delta Z$.

The change in voltage will be

$$V_A - V_{A'} = \frac{V}{1+\frac{Z_2}{Z_3}} - \frac{V}{1+\frac{Z_2'}{Z_3}} = V \cdot Z_3 \cdot \left[\frac{1}{Z_3 + Z_2} - \frac{1}{Z_3 + Z_2 + \Delta Z} \right] .$$

If we assume $\Delta Z << Z_2 + Z_3$ then the second part inside the parenthesis will be

$$\frac{1}{Z_3 + Z_2 + \Delta Z} \approx \frac{1}{Z_3 + Z_2} - \frac{1}{(Z_3 + Z_2)^2} \cdot \Delta Z \quad \text{and}$$

$$V_A - V_{A'} \approx \frac{V \cdot Z_3}{(Z_2 + Z_3)^2} \cdot \Delta Z \ .$$

Appendix B

The circuit layout.

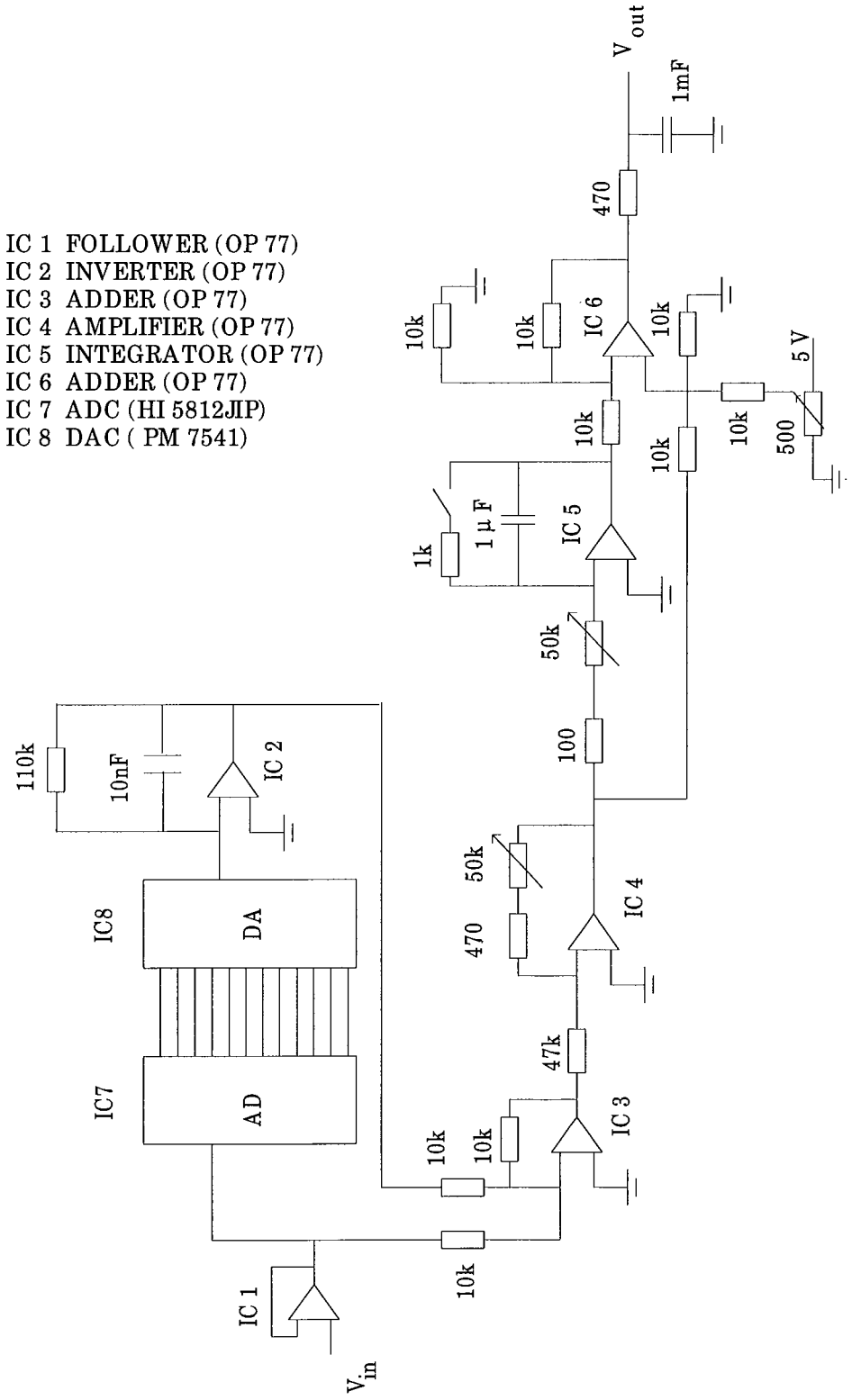

Appendix C

A calculation of the change in capacitance when scanning in x or y direction due to the angled electrodes (cf. Sect. 3.1.1).

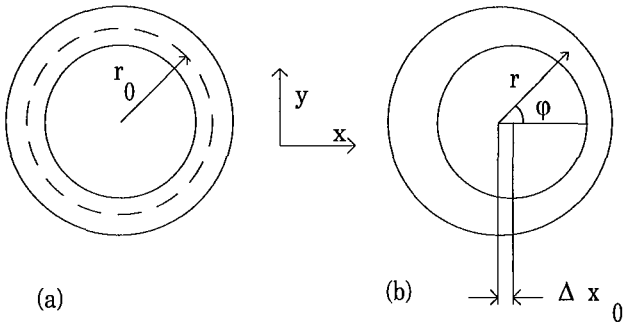

Fig. C1. The electrodes viewed from above.

In Fig C1, r_0 is the radius of the electrode and r is the radius after a small scan.

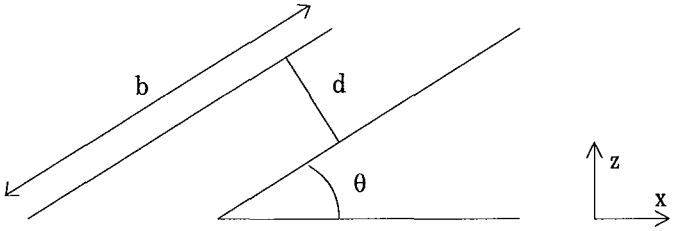

Fig. C2. A close-up on the electrodes (view from the side).

In Fig. C2, b is the width of the circular electrode, d the distance between the electrodes and θ the angle of the electrodes.
It can be seen in Fig. C2 that the change in d, Δd will be $\Delta d = \Delta x \cdot \sin(\theta)$ If we assume a maximum scan length Δx_0=5 μm ($\Delta x_0 << r_0$) we will get

$$\Delta x(\varphi) = \Delta x_0 \cdot \cos(\varphi) \qquad \text{and}$$

$$d = d_0 - \Delta x_0 \cdot \sin(\theta) \cdot \cos(\varphi) \, .$$

The distance r in Fig. C1 (b) will also be angular dependant according to

$$r(\varphi) = r_0 + \Delta x_0 \cdot \cos(\varphi) \, .$$

When being in the centre as in Fig. C1 (a), the capacitance is

$$C_0 = \varepsilon_0 \cdot \frac{A}{d} = \varepsilon_0 \cdot \int_0^{2\pi} \frac{b \cdot r_0 \cdot d\varphi}{d_0} = \varepsilon_0 \cdot \frac{2 \cdot \pi \cdot b \cdot r_0}{d_0}.$$

After scanning a distance Δx_0 in the x-direction the new capacitance will be

$$C = \varepsilon_0 \cdot \frac{A}{d} = 2 \cdot \varepsilon_0 \cdot \int_0^{\pi} \frac{b \cdot (r_0 + \Delta x_0 \cdot \cos(\varphi)) \cdot d\varphi}{(d_0 - \Delta x_0 \cdot \cos(\varphi) \cdot \sin(\theta))} =$$

$$C = 2 \cdot \varepsilon_0 \cdot b \cdot \left(r_0 \cdot \int_0^{\pi} \frac{d\varphi}{(d_0 - \Delta x_0 \cdot \cos(\varphi) \cdot \sin(\theta))} + \Delta x_0 \cdot \int_0^{\pi} \frac{\cos(\varphi) \cdot d\varphi}{(d_0 - \Delta x_0 \cdot \cos(\varphi) \cdot \sin(\theta))} \right).$$

The second integral can be solved with partial integration, resulting in the expression

$$C = 2 \cdot \varepsilon_0 \cdot b \cdot \left(-\frac{\pi}{\sin(\theta)} + \left(r_0 + \frac{d_0}{\sin(\theta)} \right) \cdot \int_0^{\pi} \frac{d\varphi}{(d_0 - \Delta x_0 \cdot \cos(\varphi) \cdot \sin(\theta))} \right).$$

This integral can be found in tables of integrals and the solution is

$$C = 2 \cdot \pi \cdot \varepsilon_0 \cdot b \cdot r_0 \cdot \left(-\frac{1}{\sin(\theta) \cdot r_0} + \left(1 + \frac{d_0}{\sin(\theta) \cdot r_0} \right) \cdot \frac{1}{\sqrt{\left((d_0)^2 - (\Delta x_0 \cdot \sin(\theta))^2 \right)}} \right).$$

If we assume an angle θ=17° (our microscope objective), a distance d_0=50 μm, a scan-length Δx_0=5 μm and a radius r_0=3 mm, then

$$\frac{C}{C_0} = 1.000468.$$

Thus, a 5 μm scan in the x-direction results in an apparent change in vertical distance of $0.000468 \cdot 50 \cdot 10^{-6} = 23\text{nm}$. This problem can easily be circumvented by using flat electrodes as discussed in Sect. 3.1.1.

Appendix D

Instruction manual.

1. Connect the cables from the bridge unit to the lock-in amplifier. It is important that the cable marked A is connected to the A input and the B cable to the B input.
Connect the oscillator output on the lock-in to the BNC contact on the bridge unit.

2. Connect the lock-in output to the control unit input and the piezo amplifiers z-input to the control unit output. Make sure that the manual adjustment knob on the amplifier is set to zero.

3. The lock-in oscillator should be set on 10 kHz and maximum amplitude. Set the phase at 0^{o}.

4. Set the lock-in on difference voltage mode (V_A-V_B) and choose the 1 mV range. The time constant should be 1 ms and the filter slope 12 dB.

5. Adjust the trim capacitance on the bridge until a small positive voltage is reached on the lock in amplifier.

6. Activate the control unit. Set the unit in adjust mode in order to adjust the distance. The distance between sample and probe can be adjusted with the knob marked adjust. When you are satisfied with the adjustments set the switch in hold mode. The control unit will now compensate for distance fluctuations.

If you wish to change the proportional gain or the integral time-constant this can be done by opening the control unit. Inside there will be two adjustment screws marked P and I. The one marked P adjusts the proportional gain and the one marked I the time-constant. Make sure you do not touch the two unmarked screws. They are used to the reference voltage.

If it is not possible to calibrate the bridge the fixed capacitances can be changed. Make sure to use capacitors with a small temperature coefficient (30 ppm).

References

1. E. Hecht, *Optics*, (Addison-Wesley, London, 1987), Chap. 10, p. 422.

2. A. G. Michette, "X-ray microscopy", Rep. Prog. Phys. **51**, 1525, (1988).

3. M. J. Dykstra, *Biological Electron Microscopy*, (Plenum Press, New York, 1992).

4. G. Binnig, C. F. Quate, and Ch. Gerber, "Atomic Force Microscopy", Phys. Rev. Lett. **12**, 930 (1986).

5. G. Binnig, H. Rohrer, Ch. Gerber, and E. Weibel, "7 × 7 Reconstruction on Si(111) Resolved in Real Space", Phys. Rev. Lett. **2**, 120 (1983).

6. E. Betzig and J. K. Trautman, "Near-field optics: microscopy, spectroscopy, and surface modification beyond the diffraction limit", Science, **257**, 189 (1992).

7. L. Malmkvist and H. M. Hertz, "Trapped particle optical microscopy", Opt. Commun. **94**, 19 (1992).

8. L. Malmkvist and H. M. Hertz, "Two-color trapped particle optical microscopy", Opt. Lett. **19**, 853 (1994).

9. L. Malmkvist and H. M. Hertz, "Second-harmonic generation in optically trapped non-linear particles using pulsed lasers", submitted to Appl. Opt.

10. The spectra is recorded by Akustikgruppen, Malmö.

11. A. E. Holman, W. C. Heerens and F. Tuinstra, "Using capacitive sensors for in situ calibration of displacements in a piezo-driven translation stage of an STM", Sensors and Actuators **A 36**, 37 (1993).

12. *Handbook of Chemistry and Physics*, 54th edition, (CRC-press, Cleveland, 1973), p. D-222.

13. L. Grahm, H. G. Jubrink, A. Lauber, *Modern Elektrisk Mätteknik del 2*, (Teknikinformation, Lund, 1992), p. 96.

14. D. J. Shaw, *Introduction to Colloid and Surface Chemistry, Fourth edition*, (Butterworth-Heinemann, Oxford, 1992), Chap. 7.

15. A. J. Bard, L. R. Faulkner, *Electrochemical Methods*, (John Wiley & Sons, New York, 1980), Chap. 1, p. 8.

16. G. Johansson, Dep. of Analytical chemistry, Lund, personal communication.

17. C. Nordling and J. Östman, *Physics Handbook*, (Studentlitteratur, Lund, 1987).

18. *Optics Guide 5*, (Melles Griot, 1990), p. 3-19.

19. S. Harb, S. T. Smith, and D. G. Chetwynd, "Subnanometer behaviour of a capacitive feedback, piezoelectric displacement actuator", Rev. Sci. Instrum. **63**, 1680 (1992).

20. T. Glad, L. Ljung, *Reglerteknik Grundläggande Teori*, (Studentlitteratur, Lund, 1989).

21. L. Grahm, H. G. Jubrink, A. Lauber, *Modern Elektrisk Mätteknik del 1*, (Teknikinformation, 1992), p. 91.

22. L. Påhlsson, "Development and fabrication of control, regulation and drive electronics for an Atomic Force Microscope", Diploma paper (Dep. of Solid State Physics, Lund, Sweden 1991).

23. W. C. Heerens, "Application of capacitance techniques in sensor design", Phys. E: Sci. Instrum. **19**, 897 (1986).

24. D. P. Hand, T. A. Carolan, J. S. Barton, J. D. C. Jones, "Profile measurement of optically rough surfaces by fiber-optic interferometry", Optics Lett. **18**, 1361 (1993).